Electronic Supplementary Material (ESI) for Journal of Materials Chemistry C.

Supporting Information

Photovoltage as a quantitative probe of carrier generation and recombination in organic photovoltaic cells

*Tao Zhang and Russell Holmes**

Department of Chemical Engineering and Materials Science, University of Minnesota, Minneapolis, MN 55455, United States

1. Comparison between charge extraction decay and open-circuit voltage decay

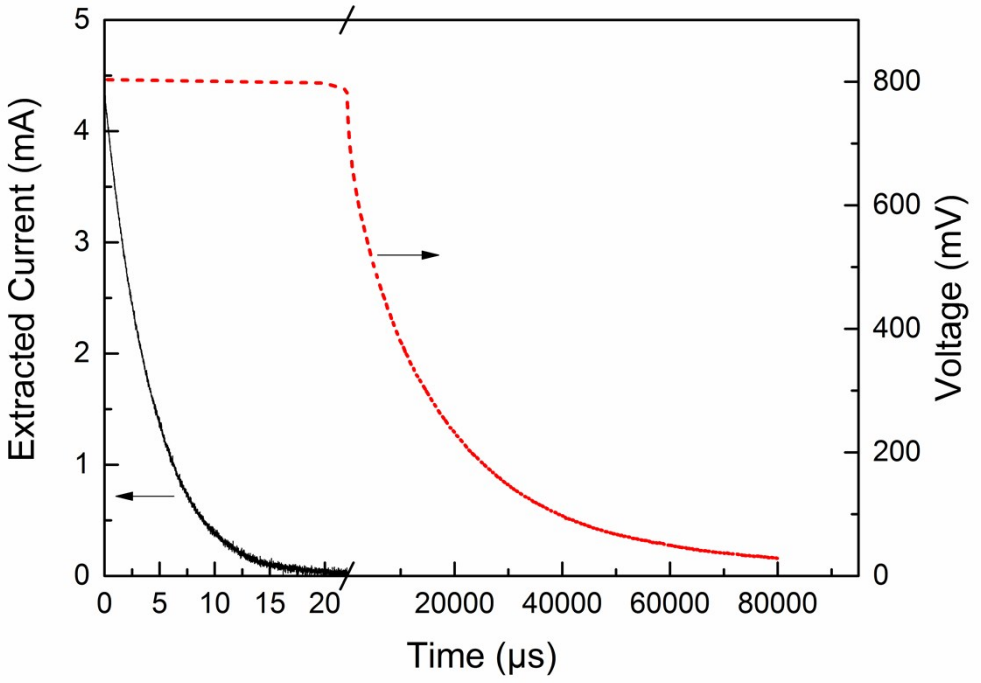

Figure S1. (Solid black line) Decay of extracted current obtained by switching the DTDCPB-C_{60} BHJ in Figure 1d from open-circuit (V_{OC} = 797 mV) to short-circuit. (Broken red line) Voltage decay (V_{OC} = 803 mV at t = 0 μs) of the DTDCPB-C_{60} BHJ device at open-circuit. The illumination to provide initial V_{OC} is turned off at t = 0 μs.

2. Lifetime of free charge carriers

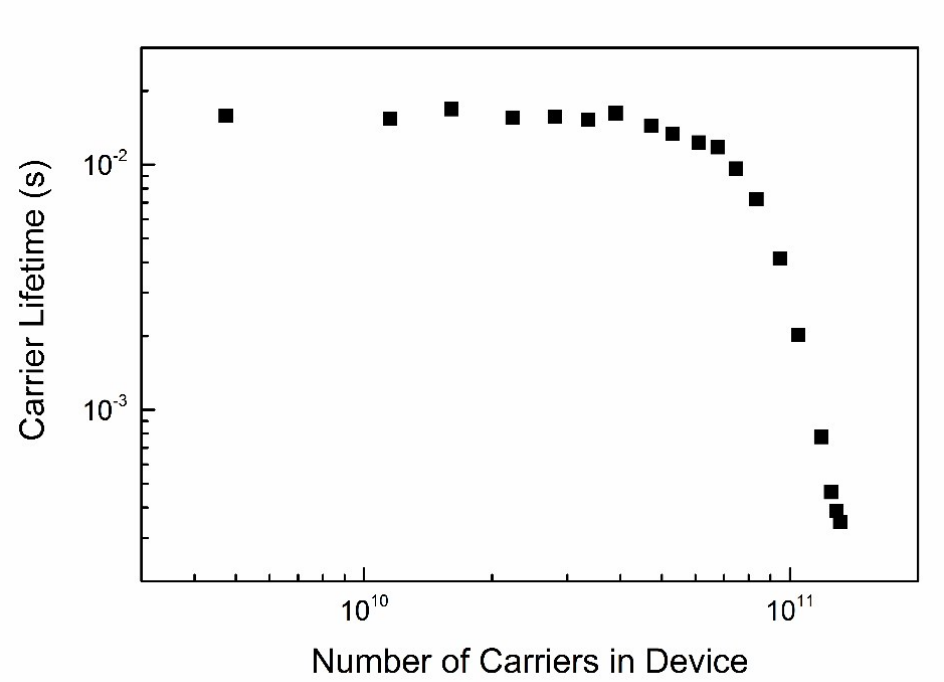

Figure S2. Carrier lifetime as a function of carrier number in DTDCPB-C_{60} BHJ. The lifetime here is derived as the ratio of carrier number to carrier recombination rate measured in Figure 3b.

2. Additional plots of carrier rise and decay

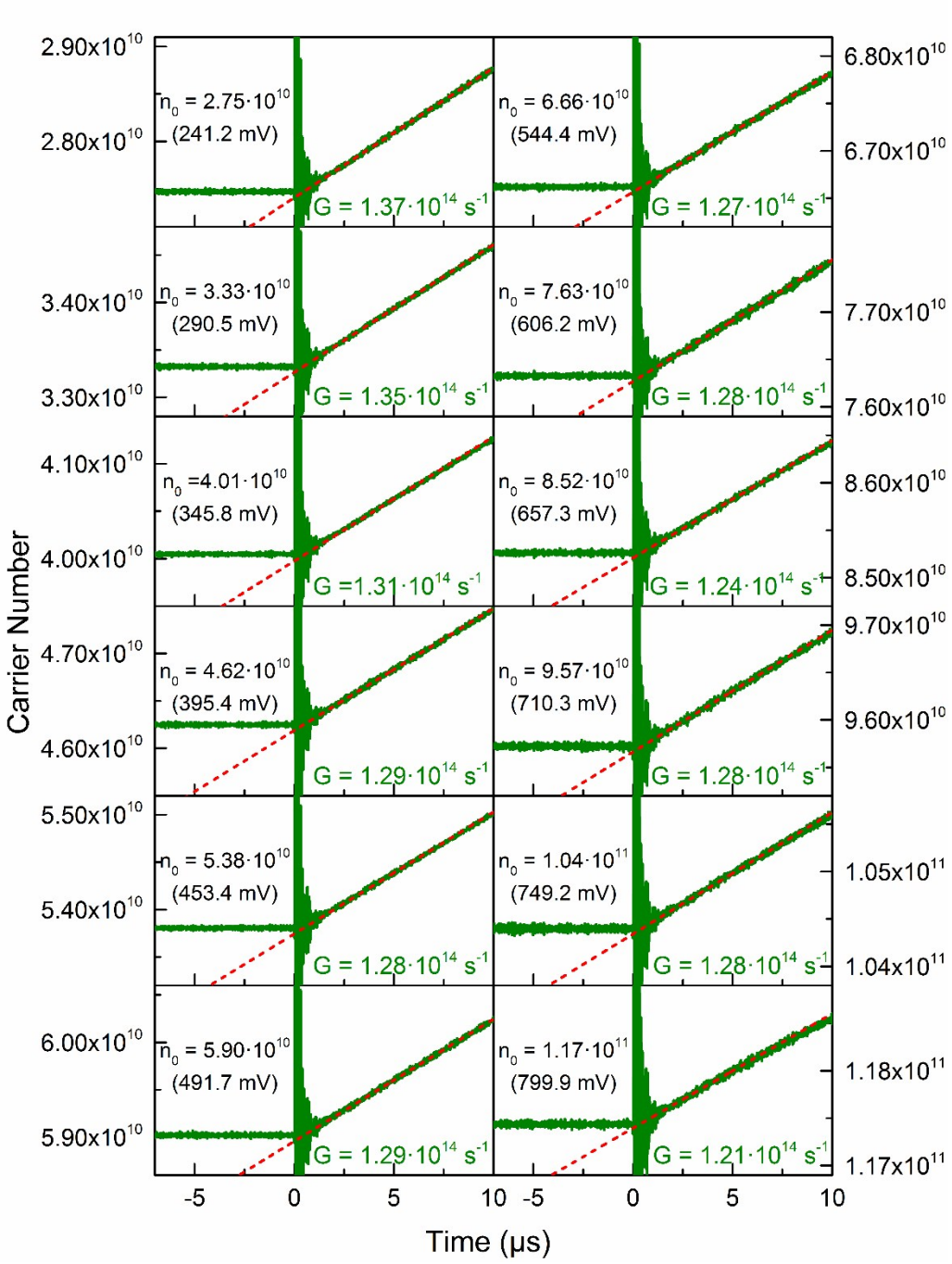

Figure S3. Plots of charge carrier rise within the device in Figure 3 versus time for measurement of carrier generation rate (G). The rates are approximated as the slope of linear rise region (first 5 us). The operating voltages (V_{OP} = 241.2 - 799.9 mV) corresponding to n_0 are shown in brackets. The device is held at steady state before t = 0 μs using constant background illumination (blue LED). A second green LED is turned on at t = 0 μs and leads to increase in carrier number stored within the device.

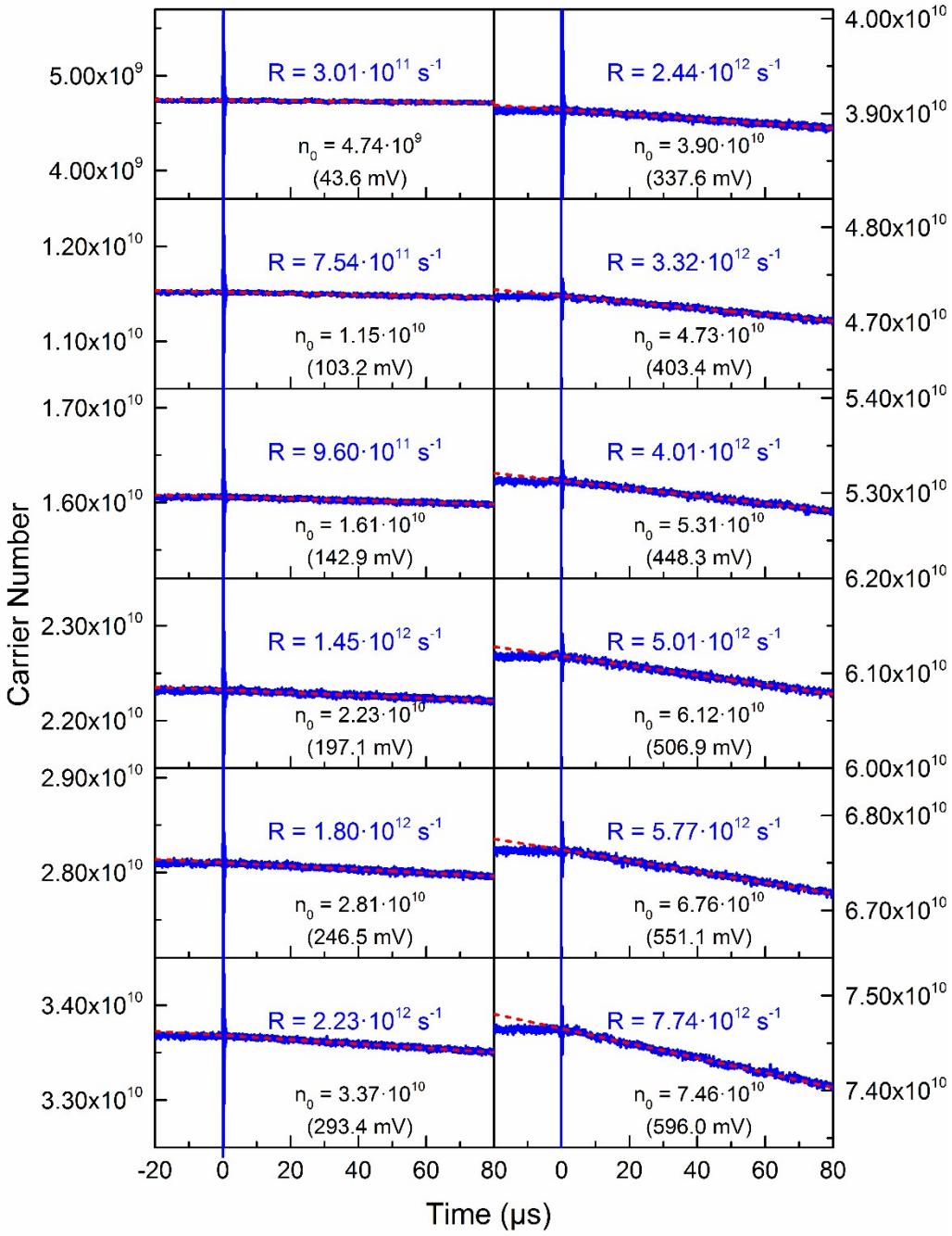

Figure S4. Plots of charge carrier decay within the device in Figure 3 (V_{OP} = 43.6 - 596.0 mV) for measurement of carrier recombination rate (R). The rates are approximated as the slope of linear decay region (first 20 us). The operating voltages correspond n_0 are shown in brackets. The device is held at steady state before t = 0 μs using constant background illumination (blue LED). Background illumination is turned off at t = 0 μs and leads to decrease in carrier number stored within the device.

4. Intensity dependent short-circuit current

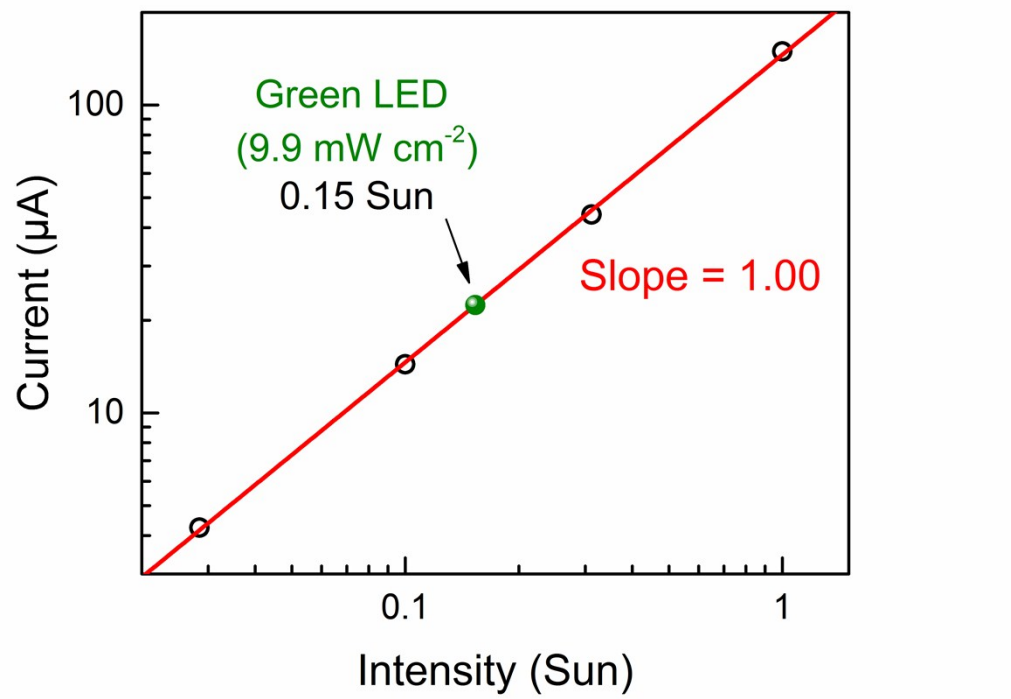

Figure S5. Short-circuit current (I_{SC}) of the DTDCPB-C_{60} BHJ in Figure 1d as a function of simulated AM1.5G light intensity (open circle) in logarithmic scale. A linear fit (solid red line) with a slope of 1.00 to the data is also shown. The I_{SC} in Figure 4 (illuminated by a green LED) is corresponding to a short-circuit current generated by 0.15 Sun simulated AM1.5G illumination.

5. Intensity dependence of extracted carriers and generation current

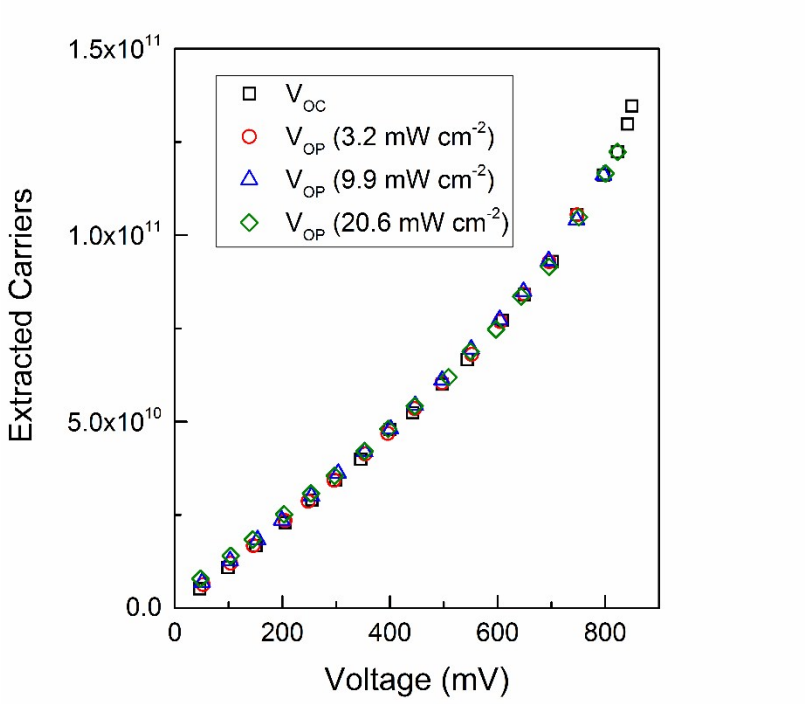

Figure S6. The number of extracted carriers as a function of open-circuit voltage (V_{OC}) and operating voltage (V_{OP}) derived by integrating current transients with respect to time.

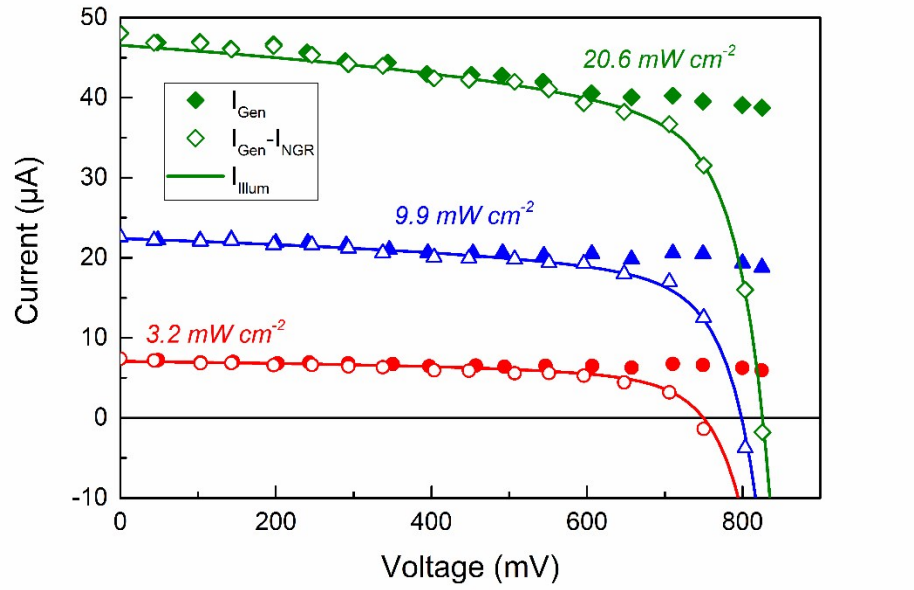

Figure S7. Generation current, illumination current and recreated illumination current using I_{NGR} from TPV measurement as a function of voltage in DTDCPB-C_{60} BHJ under green LED illumination (3.2/9.9/20.6 mW cm^{-2}).

6. Charge collection efficiency determined by reverse bias external quantum efficiencies

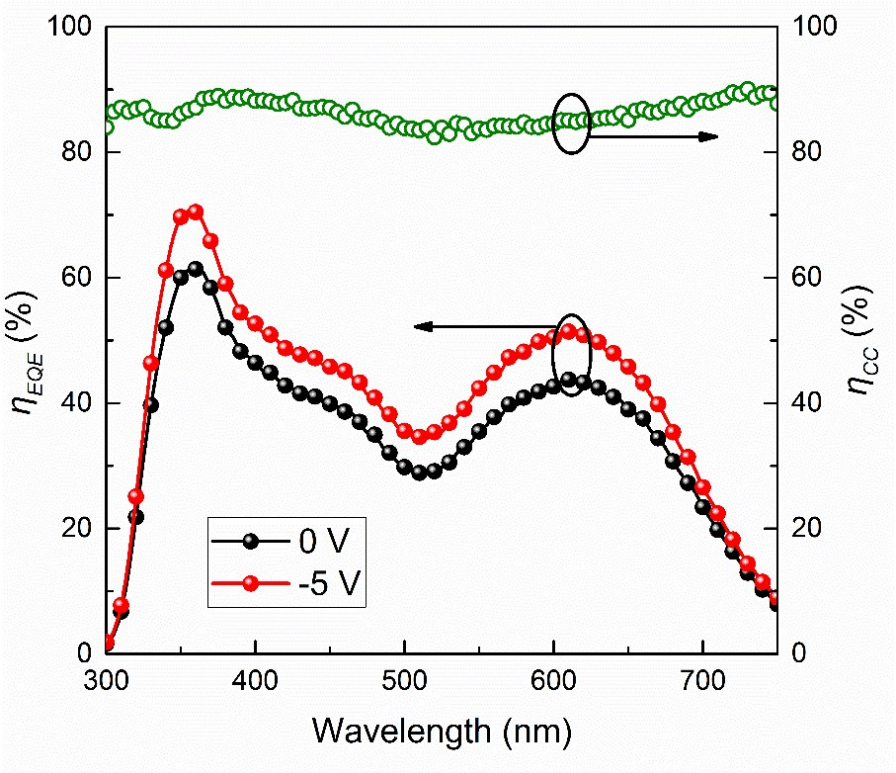

Figure S8. External quantum efficiency (η_{EQE}) of the DTDCPB-C_{60} BHJ in Figure 1d at short-circuit (black closed symbols) and -5 V (red closed symbols). The absorption efficiency (η_A) is approximated as the reverse bias η_{EQE} at -5 V. The charge collection efficiency (η_{CC}) is determined as the ratio of short-circuit η_{EQE} to η_A.

7. Comparison between I_{Gen} and I_{Illum}-I_{Dark} difference

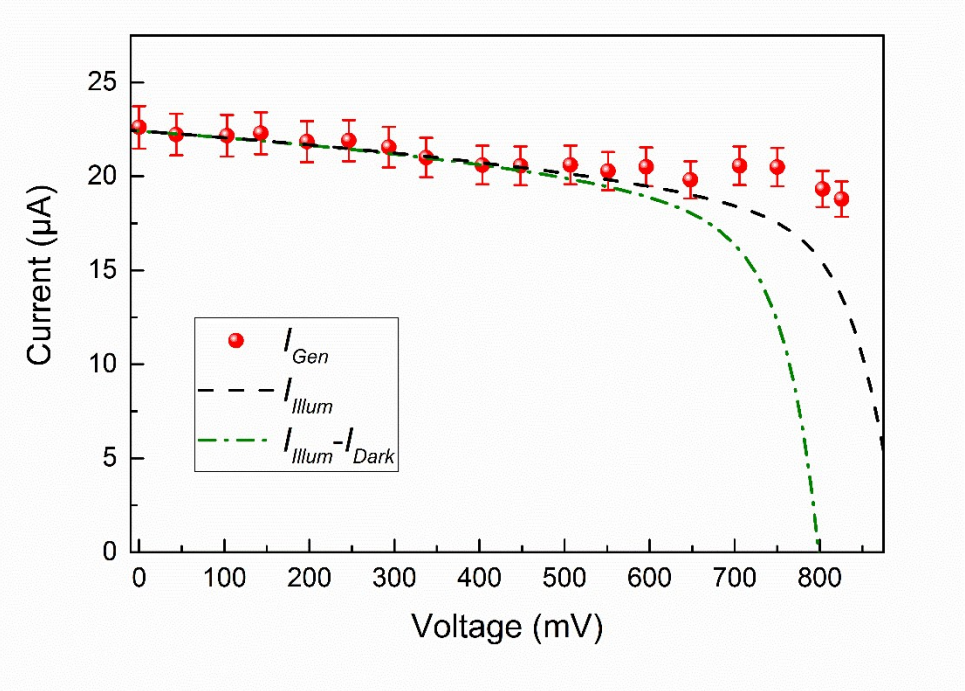

Figure S9. Carrier generation current (I_{Gen}) extracted from photovoltage measurements compared to the difference between the measured illuminated current (I_{Illum}) and dark current (I_{Dark}) of the DTDCPB-C_{60} BHJ in Figure 1d as a function of applied voltage.

To understand whether the difference between I_{Illum} and I_{Dark} is a good approximation for the I_{Gen} for the DTDCPB-C_{60} BHJ in Figure 4, both I_{Gen} (from photovoltage) and the approximate I_{Gen} (I_{Illum}-I_{Dark}) are plotted as a function of voltage in Figure S7. The I_{Illum}-I_{Dark} difference is in good agreement with the photovoltage-extracted I_{Gen} up to 600 mV, where the I_{NGR} is much lower than I_{Gen}. When the I_{NGR} increases with voltage (> 600 mV), the I_{Illum}-I_{Dark} difference is smaller than I_{Gen}. This is likely due to the increased carrier density in the active layer under illumination compared to in the dark, especially under high forward bias, which leads to a larger I_{NGR}.

8. Comparison between I_{Gen} and I_{Illum}-I_{Dark} difference

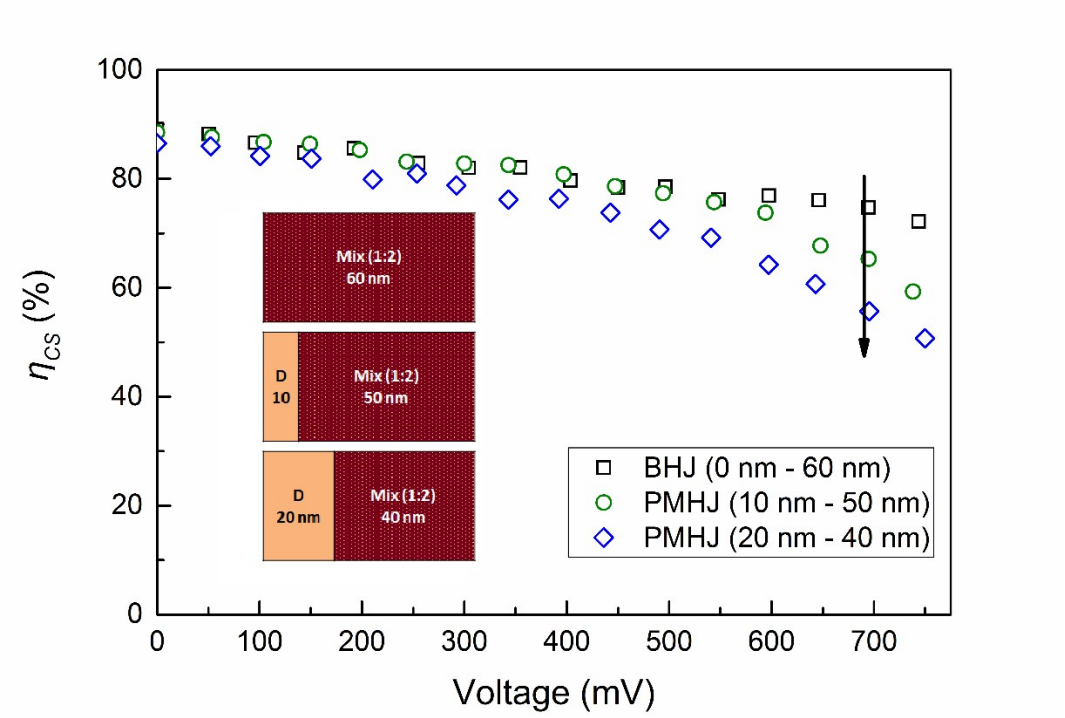

Figure S10. Charge separation efficiency (η_{CS}) of OPVs with the following structure: 10 nm MoO_x/x nm DTDCPB/ (60-x) nm DTDCPB-C_{60} (1:2) mixture/10 nm BCP/100 nm Al. The η_{CS} as a function of voltage is measured as described in main text using a blue LED (455 nm) with intensity of 14.7 mW cm^{-2}.

To understand the origin of severe geminate recombination loss in DTDCPB-C_{60} PHJ, the role of neat DTDCPB in CT state separation is examined. Figure S8 shows the charge separation efficiency (η_{CS}) of DTDCPB-C_{60} OPVs with 60-nm-thick active layer as a function of neat DTDCPB layer thickness. Blue LED illumination (mostly absorbed by C_{60}) is employed to only populate CT states in mixture. As built-in voltage (V_{bi}) is mainly determined by work function difference between electrodes, we assume change in V_{bi} is not significant as a function with neat layer thickness. The result shows that the η_{CS} decreases with DTDCPB thickness for a given applied voltage (V), especially for high forward bias, when the driving voltage (V_{bi}-V) is small. As the physical environment of CT states in mixture are the same (charge carrier mobility, lifetime of CT states and dielectric constant), η_{CS} is only depends on strength of electric field. Therefore, the decreased η_{CS} with DTDCPB thickness suggests that neat DTDCPB consume more built-in field than mixture. A thicker neat layer leads to weaker electric field at donor-acceptor interface and lower η_{CS} for the same driving voltage.

9. LED spectra

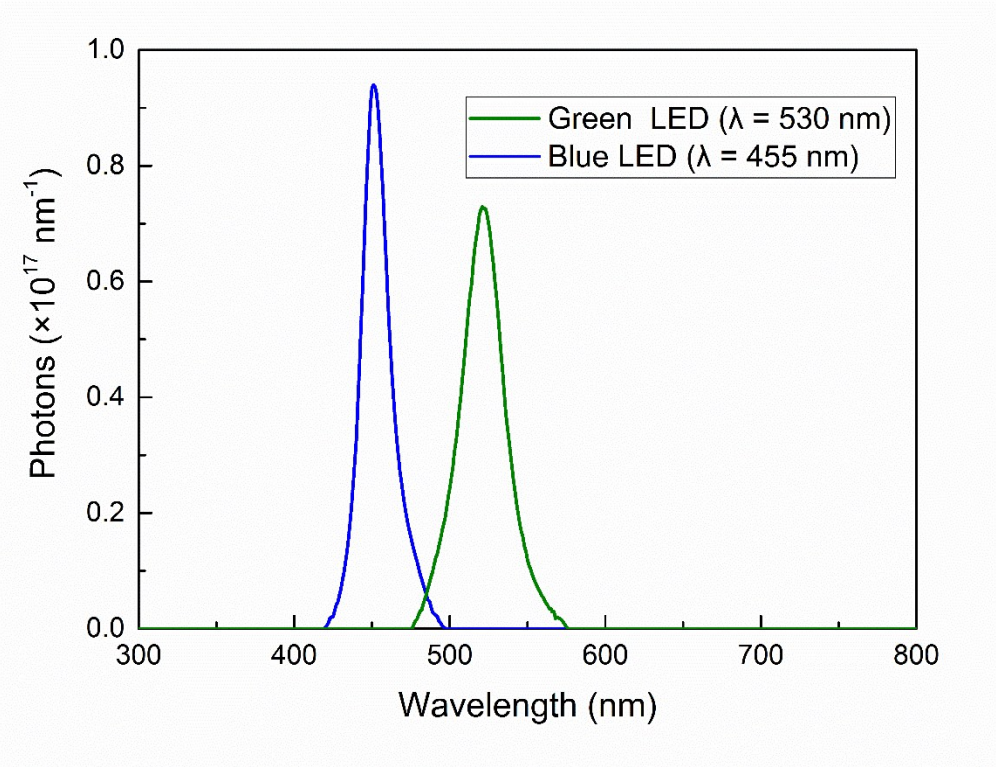

Figure S11. Pump spectra for LEDs peaked at wavelengths of λ = 455 nm (blue) and λ = 530 nm (green). The spectra are normalized to 1 W illumination through an aperture with an area of 0.0176 cm^2.

9. Device performance under 1 sun illumination

1 Sun Parameters	V_{OC} (V)	J_{SC} (mA cm^{-2})	FF	η_P (%)
DTDCPB-C_{60} BHJ	0.86	8.46	0.67	4.86
DTDCPB-C_{60} PHJ	0.80	0.82	0.22	0.15
CuPc-C_{60} PHJ	0.24	3.55	0.52	0.44

Table S1. Performance of devices in Figure 1d under simulated AM1.5G 1 Sun illumination. All devices were illuminated through an aperture with an area of 0.0176 cm^2.

The performance of devices studied in this work (AM1.5G 1 Sun) are shown in Table S1. The DTDCPB-based BHJ has been used to demonstrate high η_P (8~10%) when using C_{70} as the electron acceptor material.